

Intrinsic and extrinsic antiferromagnetic damping in NiO

Takahiro Moriyama,^{1,*} Kensuke Hayashi,² Keisuke Yamada,² Mutsuhiro Shima,² Yutaka Ohya,² and Teruo Ono¹¹*Institute for Chemical Research, Kyoto University, Gokasho, Uji, Kyoto 611-0011, Japan*²*Department of Materials Science and Processing, Graduate School of Natural Science and Technology, Gifu University, Yanagido, Gifu City, Gifu 501-1193, Japan*

(Received 13 February 2019; revised manuscript received 11 April 2019; published 9 May 2019)

In antiferromagnetic spintronics where manipulation of the antiferromagnetic spins is a central technological challenge, it is important to understand the dynamic properties, especially their THz spin dynamics and the magnetic damping. Here, we investigate thoroughly the antiferromagnetic spin dynamics in NiO by broadband THz spectroscopy and find the remarkable difference in the damping constants $\alpha = 5.0 \pm 0.4 \times 10^{-4}$ and $7.4 \pm 0.4 \times 10^{-4}$, respectively, for mono- and polycrystalline NiO, indicating the existence of strong extrinsic contributions to the damping, such as two-magnon scattering. Our results shed light on the mechanism of the antiferromagnetic dissipative dynamics and give important insights for developing antiferromagnetic and THz spintronics devices.

DOI: [10.1103/PhysRevMaterials.3.051402](https://doi.org/10.1103/PhysRevMaterials.3.051402)

Direct manipulation of the antiferromagnetic magnetization by the spin angular momentum of the electron [1,2], or the spin torque effect, possibly yields novel spintronic applications, such as THz devices [3–6], and field proof magnetic memory devices [7–11], by taking advantage of the ultrafast spin dynamics and zero net magnetization properties of antiferromagnets. In the same fashion as the spin torque phenomenology in ferromagnets [12–14], the magnetic damping is one of the most important properties which determines the performance of antiferromagnetic spin devices [3,6]. Therefore, how to characterize and understand the antiferromagnetic spin dynamics and the magnetic damping inherent in antiferromagnetic materials is becoming a central interest in antiferromagnetic spintronics.

While both experimental and theoretical investigations of antiferromagnetic resonance began in the 1950's [15–18], they have been recently revisited with more advanced experimental techniques [19–21] as well as with more rigorous theoretical treatments [22–25] in the context of emerging antiferromagnetic spintronics. Kittel [15] and Nagamiya [16] first showed that the eigenfrequency of the antiferromagnetic resonance is $\omega_r \approx \gamma \sqrt{2H_E H_A}$, where $\gamma = 1.76 \times 10^{11} (\text{T}^{-1} \text{s}^{-1})$ is the gyromagnetic ratio, H_E is the exchange field, and H_A is the uniaxial anisotropy field. Because H_E , typically $\sim 1000 \text{ T}$, comes into play in the eigenfrequency, the antiferromagnetic resonance occurs at a much higher frequency, i.e., $\sim \text{THz}$, than the ferromagnetic resonance ($\sim \text{GHz}$). Therefore, in the early stages of the investigations, state-of-art spectroscopy with a rather inefficient and weak far-infrared source [17,18] was employed to investigate various antiferromagnets, such as NiO, CoO, MnO, and Cr_2O_3 . Although their high resonant frequencies have been experimentally confirmed, the experimental technique at the time was not sufficiently sensitive to capture the resonant linewidth with which a detailed analysis

of the magnetic damping could be possible. Moreover, the importance of the magnetic damping in antiferromagnets was not seriously argued. However, owing to recent developments in the THz technologies, frequency-domain THz spectroscopies with a much better sensitivity than before have now become accessible and affordable for investigating in more detail the spin dynamics in antiferromagnets.

In this Rapid Communication, we report thorough investigations of the antiferromagnetic resonance and the damping of both monocrystalline and polycrystalline NiO, a prototypical collinear antiferromagnet widely investigated in antiferromagnetic spintronics [9,10,19–21,26,27], by employing the technology of the continuous-wave (cw) frequency-domain THz spectroscopy. The resonant linewidth analysis in the frequency-domain measurements allows us more straightforward and precise characterizations of the magnetic damping in contrast to the time-domain measurements [19–21] as well as those old technologies [18].

We made use of a cw-THz spectroscopy system [28] (with TOPTICA photonics: TeraScan 780) shown in Fig. 1(a) [see Supplemental Material (SM) for the detailed working principle [29]]. A 0.45-mm-thick monocrystalline NiO plate with a (111) cut and a 1.4-mm-thick polycrystalline NiO pellet sintered from NiO powder were employed in the measurements (see SM for the detailed sample preparation procedure). The x-ray diffraction shown in Fig. 1(b) reveals that the monocrystalline sample is fully oriented with the (111) plane and the polycrystalline sample shows random orientations of the crystal grains with a grain size of 100 nm–10 μm [30]. These samples are placed on a heater plate with an aperture positioned between the emitter and the detector. The sample temperature T was varied from 300 to 443 K. The THz wave is transmitting in the sample thickness direction. No magnetic field was applied in the measurements.

Figure 1(c) shows the transmission spectra at 305 K for the monocrystalline and the polycrystalline samples. A Fabry-Pérot (FP) interference pattern due to multireflections at the

*mtaka@scl.kyoto-u.ac.jp

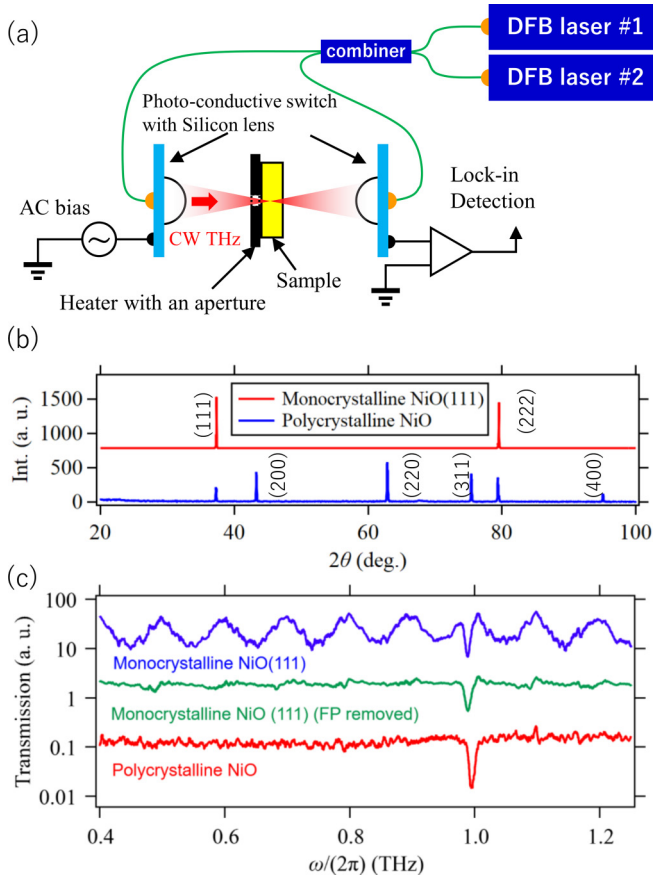


FIG. 1. THz spectroscopy measurements. (a) Schematic illustration of the cw-THz spectroscopy setup. (b) X-ray diffraction for the mono- and polycrystalline NiO samples. (c) Representative transmission spectra at 305 K for the mono- and polycrystalline samples. The spectrum in the middle is the processed data after subtraction of Fabry-Pérot interference.

front and back surfaces is observed for the monocrystalline sample as the sample is nicely cut and polished. After removing the FP pattern (see SM), a sharp absorption peak at around 1 THz is illuminated and the peak frequency is consistent with the previously reported antiferromagnetic resonance of NiO [18–20]. The polycrystalline sample also shows a peak at a similar frequency. An insignificant FP interference pattern in the polycrystalline sample could be due to rough surfaces inherent to the powder press process.

Figure 2 shows the temperature dependence of the transmission spectra and the resonant frequency for the two samples. It is clearly seen that the absorption peak shifts to lower frequency as temperature increases, which is in good agreement with previous reports [18]. No other spectral features in the range of 0.1–2 THz were seen to be strongly variant under the temperature variation [see Figs. 2(a) and 2(b)]. We note that the periodic pattern of the transmission as a function of frequency in Fig. 2(a) is due to the FP discussed above. As shown in Fig. 3, the resonant linewidth, obtained by a Lorentzian fitting, is overall greater for the polycrystalline sample and it increases with increasing temperature in both samples.

We now come to detailed discussions on the experimental results. Based on the two coupled equations of motion for uniform spin dynamics (with the magnon wave number $k = 0$) of a collinear antiferromagnet with two magnetic sublattices [24,31], the imaginary part of the frequency-dependent susceptibility χ_i which is relevant to the absorption peak is given by the Lorentzian function as (see SM for a step-by-step derivation)

$$\chi_i = \frac{\gamma M_0 \Delta\omega/2}{(\omega_0 - \omega)^2 + (\Delta\omega/2)^2}, \quad (1)$$

where ω is the excitation frequency, M_0 is the magnitude of the sublattice magnetic moment, and the resonant frequency as

$$\omega_r = 2\gamma M_0 \sqrt{K(J+K)} \approx 2\gamma M_0 \sqrt{KJ}, \quad (2)$$

where $J(>0)$ is the molecular field constant representing the exchange coupling between the sublattices and K representing the anisotropy energy constant. One can reproduce the effective fields as $H_E = JM_0$ and $H_A = 2KM_0$ so that Eq. (2) comes down to the Kittel's expression [15] with $K \ll J$: $\omega_r \approx \gamma \sqrt{2H_E H_A}$. The resonant linewidth (a full width at half maximum) $\Delta\omega$ can be written as

$$\Delta\omega = 2\gamma M_0 (J + 2K)\alpha \approx 2\gamma M_0 J\alpha. \quad (3)$$

It should be noted that, in contrast to the case of a ferromagnetic resonance linewidth where $\Delta\omega \approx \gamma H_A \alpha$ with a typical anisotropy field $H_A < 1$ T, the resonant linewidth for antiferromagnets has a much larger coefficient $M_0 J$ which is typically ~ 1000 T [32].

Since the molecular field constant J is nearly independent of temperature, possible quantities giving rise to the temperature-dependent resonant frequency are M_0 and K . As the magnetic anisotropy constant is expected to vary with a power of sublattice magnetization [18], we fit the temperature dependence of the resonant frequency with a power of a Brillouin function $B_S(T)$ with $S = 1$ appropriate for the Ni^{2+} sublattice magnetization. More explicitly, the resonance data were fitted with the equation $\omega = \omega_0 [M'_0(T)]^n$, where ω_0 is the resonant frequency at 0 K and $M'_0(T)$ is the normalized sublattice magnetization computed by $B_{S=1}(T)$. As shown in Figs. 2(c) and 2(d), the fitting with the exponent $n = 0.72$ results in a reasonable Néel temperature T_N for NiO (reportedly $T_N = 523$ K [33]) in contrast to the molecular field approximation ($n = 1$) and the empirical exponent ($n = 1/2$) [34]. Both polycrystalline and monocrystalline samples show quite similar fitting results with $\omega_0/(2\pi) \sim 1.1$ THz, suggesting that the molecular field, the anisotropy, and their temperature dependences are robust regardless of the mono- or polycrystallinity of the sample.

On the other hand, the resonant linewidths $\Delta\omega$ are found to be greater in the polycrystalline sample, as shown in Fig. 3(c). The linewidths are $\Delta\omega/(2\pi) = 9.8 \pm 0.6$ and 14.6 ± 0.6 GHz at 302 K for the mono- and polycrystalline samples, respectively. The molecular field constant J can be estimated by $J = 1/\chi_\perp$, where $\chi_\perp = (3/2)\chi$ is the perpendicular magnetic susceptibility with a susceptibility of random orientations χ at low temperature [34,35]. With the experimentally obtained $\chi = 6.11 \pm 0.01 \times 10^{-4}$ (see SM for more information) and $M_0 = 0.32$ T [36] for both samples,

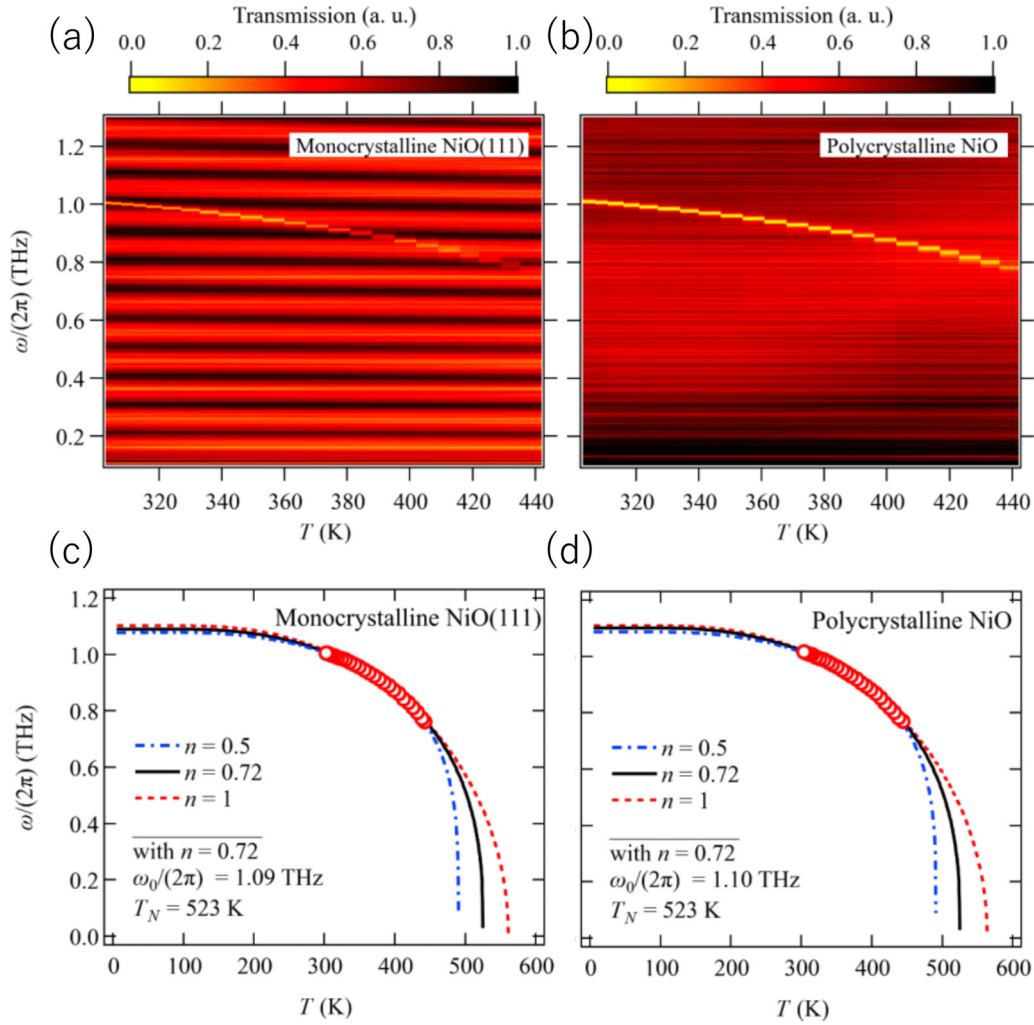


FIG. 2. Transmission spectra as a function of temperature (a) for the monocrystalline sample and (b) for the polycrystalline sample, and the resonant frequency as a function of temperature (c) for the monocrystalline sample and (d) for the polycrystalline sample. Open circles are the experimental data and the solid, dotted, and dashed lines are the fitting.

Eq. (3) yields $\alpha = 5.0 \pm 0.4 \times 10^{-4}$ and $7.4 \pm 0.4 \times 10^{-4}$, respectively, for mono- and polycrystalline samples. These small α are certainly appealing for spintronic applications and are reasonably close to previously reported values obtained by the time-domain technique [19]. On the other hand, the remarkable difference of α in mono- and polycrystalline samples strongly manifests extrinsic contributions to the damping. It is also more interesting to find the temperature dependence of $\Delta\omega/(2\pi)$. $\Delta\omega/(2\pi)$ in the polycrystalline sample increases much more rapidly with increasing temperature than that in the monocrystalline sample. According to Eq. (3), M_0 is the only temperature-dependent quantity but it basically decreases with increasing temperature in accordance with $B_{S=1}(T)$. Therefore, this temperature dependence of $\Delta\omega/(2\pi)$ is also an indication of additional contributions which were not considered in the above derivation of the antiferromagnetic dynamics.

Given that comprehensive microscopic theories are still not available for both intrinsic and extrinsic damping of antiferromagnetic spin dynamics of interest, we presume that spin relaxation processes similar to the ferromagnetic case would

be present in antiferromagnets. Therefore, typical relaxation processes can be considered via spin-spin, spin-lattice, and spin-electron interactions [31]. While spin-electron interactions should be least relevant for the present case of the insulating antiferromagnetic NiO, spin-lattice and spin-spin interactions can be main contributors. A dominant source of intrinsic damping is the spin-lattice interaction via a strong magnetoelastic coupling in NiO [37]. On the other hand, extrinsic damping can possibly come from both spin-lattice and spin-spin interactions via any nonuniform crystallinity as well as nonuniform magnetic properties within the sample, e.g., defects, grain boundaries, and distributions of the anisotropy magnitude, which are obviously more significant in the polycrystalline case. We note that, however, the distribution of the anisotropy *direction*, as it is the simplest cause for the emergence of extrinsic linewidth broadening in ferromagnets, should not take effect in the present case since no applied external field breaks symmetry in the resonant excitations in each magnetic domain (or crystal grain).

In a similar fashion to the case of ferromagnetic resonance, two-magnon scattering should primarily be considered to

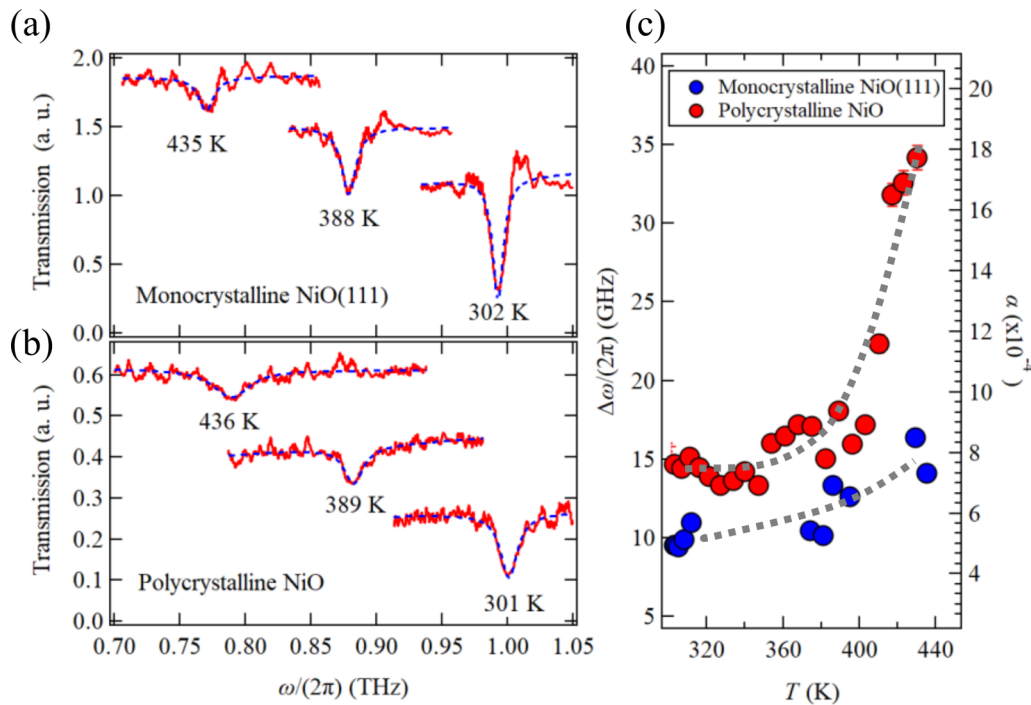


FIG. 3. Resonant linewidths and the damping α . Representative absorption lines at various temperatures for (a) the monocrystalline sample and (b) the polycrystalline sample. The dotted curves are the Lorentzian fitting to extract the resonant linewidth $\Delta\omega$. (c) $\Delta\omega/(2\pi)$ and α as a function of temperature for the mono- and polycrystalline samples. Note that some data points are missing for the monocrystalline sample because transmission minima due to the Fabry-Pérot interference smear the antiferromagnetic resonant absorption peak, making the linewidth characterization impossible. The uncertainty of the linewidth and α originates from the uncertainty of the Lorentzian peak fitting. The dotted curves are guides for the eye.

interpret the extrinsic damping in antiferromagnets [38]. In fact, two-magnon scattering has been observed with Raman spectroscopy in a variety of antiferromagnetic materials [39], albeit at a much higher energy ($\sim 1400 \text{ cm}^{-1} \equiv 42 \text{ THz}$) than our present case. In the present case of the antiferromagnetic spin dynamics of a uniform mode ($k = 0$), we can similarly interpret that the uniform mode is scattered by two magnon modes with $k \neq 0$, leading to an additional energy dissipation, therefore an additional damping for the uniform mode at which we are looking. If we presume that the magnetic and crystalline nonuniformity increase the scattering cross section of the two-magnon process in the same manner as the ferromagnetic case [38], it is quite natural to have a larger extrinsic damping in the polycrystalline sample. The temperature dependence of $\Delta\omega$ can also be simply explained by the increase of the scattering cross section with increasing temperature, as is the case for Raman spectroscopy [39]. The drastic increase of $\Delta\omega/(2\pi)$ suggests the rapid increase of the two-magnon process with increasing temperature in the polycrystalline sample. Further quantitative arguments certainly require extensive development of a microscopic theoretical model for spin dynamics in antiferromagnetic textures.

In summary, we investigated the temperature dependence of antiferromagnetic resonance and the damping in poly- and

monocrystalline NiO. The resonant frequency ($\sim 1 \text{ THz}$ at room temperature) was found to decrease with increasing temperature, which was nicely explained by the temperature dependence of the anisotropy with a power of the sublattice magnetization with the exponent $n = 0.72$. We also found the damping parameters to be $\alpha = 5.0 \pm 0.4 \times 10^{-4}$ and $7.4 \pm 0.4 \times 10^{-4}$ for the mono- and polycrystalline samples, respectively. The remarkable difference in α depending on the crystallinity manifests the significance of the extrinsic damping in antiferromagnets. We also speculated that the temperature dependence of the damping can be attributed to the extrinsic damping induced by two-magnon scattering. Although the lack of a microscopic theoretical model prevents further qualitative arguments, our thorough experimental results will shed light on the long-abandoned physics of the antiferromagnetic dissipative dynamics and give important insights for developing antiferromagnetic and THz spintronics devices.

This work was supported in part by JSPS KAKENHI Grants No. 17H04924, No. 15H05702, No. 17H04795, No. 18H01859, and No. 17H05181 (“Nano Spin Conversion Science”), and by the Collaborative Research Program of Institute for Chemical Research, Kyoto University (Grant No. 2018-61).

[1] T. Jungwirth, X. Marti, P. Wadley, and J. Wunderlich, *Nat. Nanotechnol.* **11**, 231 (2016).

[2] V. Baltz, A. Manchon, M. Tsoi, T. Moriyama, T. Ono, and Y. Tserkovnyak, *Rev. Mod. Phys.* **90**, 015005 (2018).

- [3] R. Cheng, J. Xiao, Q. Niu, and A. Brataas, *Phys. Rev. Lett.* **113**, 057601 (2014).
- [4] J. Walowski and M. Münzenberg, *J. Appl. Phys.* **120**, 140901 (2016).
- [5] D. M. Mittleman, *J. Appl. Phys.* **122**, 230901 (2017).
- [6] R. Khymyn, I. Lisenkov, V. Tiberkevich, B. A. Ivanov, and A. Slavin, *Sci. Rep.* **7**, 43705 (2017).
- [7] P. Wadley, B. Howells, J. Elezny, C. Andrews, V. Hills, R. P. Campion, V. Novak, K. Olejnik, F. Maccherozzi, S. S. Dhesi, S. Y. Martin, T. Wagner, J. Wunderlich, F. Freimuth, Y. Mokrousov, J. Kune, J. S. Chauhan, M. J. Grzybowski, A. W. Rushforth, K. W. Edmonds, B. L. Gallagher, and T. Jungwirth, *Science* **351**, 587 (2016).
- [8] T. Kosub, M. Kopte, R. Hühne, P. Appel, B. Shields, P. Maletinsky, R. Hübner, M. O. Liedke, J. Fassbender, O. G. Schmidt, and D. Makarov, *Nat. Commun.* **8**, 13985 (2017).
- [9] X. Z. Chen, R. Zarzuela, J. Zhang, C. Song, X. F. Zhou, G. Y. Shi, F. Li, H. A. Zhou, W. J. Jiang, F. Pan, and Y. Tserkovnyak, *Phys. Rev. Lett.* **120**, 207204 (2018).
- [10] T. Moriyama, K. Oda, T. Ohkochi, M. Kimata, and T. Ono, *Sci. Rep.* **8**, 14167 (2018).
- [11] T. Moriyama, W. Zhou, T. Seki, K. Takanashi, and T. Ono, *Phys. Rev. Lett.* **121**, 167202 (2018).
- [12] J. C. Slonczewski, *J. Magn. Magn. Mater.* **159**, L1 (1996).
- [13] L. Berger, *Phys. Rev. B* **54**, 9353 (1996).
- [14] D. C. Ralph and M. D. Stiles, *J. Magn. Magn. Mater.* **320**, 1190 (2008).
- [15] C. Kittel, *Phys. Rev.* **82**, 565 (1951).
- [16] T. Nagamiya, *Prog. Theor. Phys.* **6**, 342 (1951).
- [17] L. R. Maxwell and T. R. McGuire, *Rev. Mod. Phys.* **25**, 279 (1953).
- [18] M. Tinkham, *J. Appl. Phys.* **33**, 1248 (1962).
- [19] T. Kampfrath, A. Sell, G. Klatt, A. Pashkin, S. Meahrlein, T. Dekorsy, M. Wolf, M. Fiebig, A. Leitenstorfer, and R. Huber, *Nat. Photonics* **5**, 31 (2011).
- [20] T. Satoh, S.-J. Cho, R. Iida, T. Shimura, K. Kuroda, H. Ueda, Y. Ueda, B. A. Ivanov, F. Nori, and M. Fiebig, *Phys. Rev. Lett.* **105**, 077402 (2010).
- [21] Z. Wang, S. Kovalev, N. Awari, M. Chen, S. Germanskiy, B. Green, J.-C. Deinert, T. Kampfrath, J. Milano, and M. Gensch, *Appl. Phys. Lett.* **112**, 252404 (2018).
- [22] K. M. D. Hals, Y. Tserkovnyak, and A. Brataas, *Phys. Rev. Lett.* **106**, 107206 (2011).
- [23] Q. Liu, H. Y. Yuan, K. Xia, and Z. Yuan, *Phys. Rev. Mater.* **1**, 061401 (2017).
- [24] A. Kamra, R. E. Troncoso, W. Belzig, and A. Brataas, *Phys. Rev. B* **98**, 184402 (2018).
- [25] H. Y. Yuan, Q. Liu, K. Xia, Z. Yuan, and X. R. Wang, [arXiv:1801.00217](https://arxiv.org/abs/1801.00217).
- [26] H. Wang, C. Du, P. C. Hammel, and F. Yang, *Phys. Rev. Lett.* **113**, 097202 (2014).
- [27] T. Moriyama, S. Takei, M. Nagata, Y. Yoshimura, N. Matsuzaki, T. Terashima, Y. Tserkovnyak, and T. Ono, *Appl. Phys. Lett.* **106**, 162406 (2015).
- [28] A. Roggenbuck, H. Schmitz, A. Deninger, I. C. Cámara Mayorga, J. Hemberger, R. Güsten, and M. Grüninger, *New J. Phys.* **12**, 043017 (2010).
- [29] See Supplemental Material at <http://link.aps.org/supplemental/10.1103/PhysRevMaterials.3.051402> for extensive descriptions and data.
- [30] We characterized the crystal grain size by the XRD as well as the microscope observation. See SM for more information.
- [31] A. G. Gurevich and G. A. Melkov, *Magnetization Oscillations and Waves* (CRC Press, Boca Raton, FL, 1996).
- [32] S. M. Rezende, R. L. Rodríguez-Suárez, and A. Azevedo, *Phys. Rev. B* **93**, 054412 (2016).
- [33] H. Kondoh, E. Uchida, Y. Nakazumi, and T. Nagamiya, *J. Phys. Soc. Jpn.* **13**, 579 (1958).
- [34] A. Sievers and M. Tinkham, *Phys. Rev.* **129**, 1566 (1963).
- [35] S. Chikazumi, *Physics of Ferromagnetism* (Oxford University Press, New York, 2009).
- [36] M. T. Hutchings and E. J. Samuelsen, *Phys. Rev. B* **6**, 3447 (1972).
- [37] E. Aytan, B. Debnath, F. Kargar, M. M. Lacerda, J. X. Li, S. Su, R. Lake, J. Shi, and A. A. Balandin, *Appl. Phys. Lett.* **111**, 252402 (2017).
- [38] R. Arias and D. L. Mills, *Phys. Rev. B* **60**, 7395 (1999).
- [39] M. G. Cottam, *J. Phys. C: Solid State Phys.* **5**, 1461 (1972).